Neural networks with excitatory and inhibitory components: Direct and inverse problems by a mean-field approach

Neural networks with excitatory and inhibitory components: Direct and inverse problems by a mean-field approach

Matteo di Volo,[1,2,3,*] Raffaella Burioni,[4,5,†] Mario Casartelli,[4,5,‡] Roberto Livi,[2,6,7,8,§] and Alessandro Vezzani[4,9,‖]

[1]*Group for Neural Theory, Departément des Etudes Cognitives, Ecole Normale Supérieure, Paris, France*
[2]*Centro Interdipartimentale per lo Studio delle Dinamiche Complesse, via Sansone 1, 50019 Sesto Fiorentino, Italy*
[3]*Indiana University–Purdue University, Indianapolis, Indiana 46202, USA*
[4]*Dipartimento di Fisica e Scienza della Terra, Università di Parma, via G.P. Usberti 7/A, 43124 Parma, Italy*
[5]*INFN, Gruppo Collegato di Parma, via G.P. Usberti 7/A, 43124 Parma, Italy*
[6]*Dipartimento di Fisica, Università di Firenze, via Sansone 1, 50019 Sesto Fiorentino, Italy*
[7]*Istituto dei Sistemi Complessi, CNR, via Madonna del Piano 10, 50019 Sesto Fiorentino, Italy*
[8]*INFN Sez. Firenze, via Sansone 1, 50019 Sesto Fiorentino, Italy*
[9]*S3, CNR Istituto di Nanoscienze, Via Campi 213A, 41125 Modena, Italy*

(Received 29 July 2015; revised manuscript received 30 October 2015; published 13 January 2016)

We study the dynamics of networks with inhibitory and excitatory leak-integrate-and-fire neurons with short-term synaptic plasticity in the presence of depressive and facilitating mechanisms. The dynamics is analyzed by a heterogeneous mean-field approximation, which allows us to keep track of the effects of structural disorder in the network. We describe the complex behavior of different classes of excitatory and inhibitory components, which give rise to a rich dynamical phase diagram as a function of the fraction of inhibitory neurons. Using the same mean-field approach, we study and solve a global inverse problem: reconstructing the degree probability distributions of the inhibitory and excitatory components and the fraction of inhibitory neurons from the knowledge of the average synaptic activity field. This approach unveils new perspectives on the numerical study of neural network dynamics and the possibility of using these models as a test bed for the analysis of experimental data.

DOI: 10.1103/PhysRevE.93.012305

I. INTRODUCTION

Many brain activities emerge as the combined effect of excitatory and inhibitory components associated with synaptic plasticity [1–6]. In mammalians, the fraction of inhibitory neurons is close to 20%—30% [7], and it seems plausible that this value was determined by evolutionary constraints, aiming at the effectiveness of brain functions. Recently, an explanation was proposed referring to the possibility that such a rate between inhibitory and excitatory neurons could optimize the performance of a neural network [8]. Neurons in the cortical area can exhibit quite complex scale-free structures, where inhibitory neurons play the role of hubs that control and moderate the action of the excitatory ones [9]. All of these considerations indicate that models of neural networks aiming at reproducing a great number of brain functions should take into account the presence of both excitatory and inhibitory neurons, organized in a suitable network [10–13].

The large number of units and the typical high density of connections in many brain areas suggest that a mean-field approach is a proper mathematical tool for understanding the large-scale dynamics of neural network models [6,14–17]. Recently, we have applied a *heterogeneous mean-field* (HMF) strategy to deal with the dynamics of an excitatory neural network. This method retains the basic information on the network topology through the probability distribution $P(\tilde{k})$ of the in-degree density $\tilde{k}$ of synaptic connections attributed to each neuron, and it allows us to build the dynamics of *classes* of neurons sharing the same in-degree density $\tilde{k}$, by suitable discretization of the dynamical rule [18]. The HMF approach is very effective in reproducing the main dynamical features of random dense networks of leaky-integrate-and-fire (LIF) excitatory neurons with synaptic short-term plasticity. In particular, the structure of quasisynchronous events and the distinction between families of locked and those of unlocked neurons, with a rich and complex phenomenology in synchronization related to the topological features of the network, are fully recovered [18].

Interestingly, the HMF approach also allows us to solve in a natural way a *global inverse problem*. This consists in recovering the unknown degree probability distribution $P(\tilde{k})$ from the knowledge of the average synaptic activity field. The method has been successfully applied to Gaussian and broad degree probability distributions of excitatory neurons, and it has been shown to be robust with respect to the introduction of noise and disorder [19].

In this paper we show that the HMF strategy can be generalized to networks of excitatory and inhibitory neurons, organized in a complex network topology, combining depressive and facilitating mechanisms. The main technical difficulty to overcome is that short-term synaptic plasticity obeys different dynamical rules for excitatory and inhibitory neurons [20,21]. Moreover, as discussed in Sec. II, one has to distinguish the dynamics of postsynaptic excitatory vs inhibitory neurons and, for both of these subclasses, the signals coming from presynaptic excitatory vs inhibitory neurons.

*mdivolo@iupui.edu
†raffaella.burioni@fis.unipr.it
‡mario.casartelli@fis.unipr.it
§livi@fi.infn.it
‖alessandro.vezzani@fis.unipr.it

A comparison between the original network dynamics and the corresponding HMF dynamics is reported in Sec. III. There we show that, even in a random network with both excitatory and inhibitory components, the HMF approach reproduces the main features of the different complex dynamical regimes.

In Sec. IV we discuss the features of the global synaptic activity fields emerging from the HMF dynamics for different values of the inhibitory fraction. In particular, we show that the system can display a quasiperiodic behavior characterized by locked and unlocked neurons or an asynchronous regime in which all neurons have different oscillation frequencies. Moreover, for a specific value of the inhibitory fraction, the system features an *optimal* synchronization regime, where all neurons display the same interspike interval.

In Sec. V we derive an approximated analytic relation between excitatory and inhibitory global synaptic activities, holding if the periodicities of the neurons are similar. We use this result to show, in Sec. VI, that the global inverse problem can be solved also for neural networks containing both excitatory and inhibitory components, with Gaussian and scale-free degree density distributions. In particular, we are able to reconstruct, from the average synaptic activity, the degree density distributions and the inhibitory fractions in a network with 10% inhibitory neurons and two Gaussian distributions $P(\tilde{k})$ for both inhibitory and excitatory components. The same holds in the case of a network with 30% inhibitory neurons generated by two $P(\tilde{k})$ scale-free distributions, with a larger average value of $\tilde{k}$ for the inhibitory components.

Conclusions and perspectives of our research are, finally, presented in Sec. VII.

II. LIF EXCITATORY AND INHIBITORY NEURONS WITH SYNAPTIC PLASTICITY

We consider a network of N neurons, either excitatory or inhibitory. Calling $v_i(t)$ the membrane potential of neuron i, its dynamics is ruled by the LIF model, i.e.,

$$\dot{v}_i(t) = a - v_i(t) + I_i^{\rm syn}(t), \tag{1}$$

where a is a common constant stimulus and $I_i^{\rm syn}(t)$ is the synaptic current coming from the connections with other neurons. All variables can be rescaled to work with adimensional units (see [18] and [19]). For instance, time is rescaled to the membrane time constant $\tau_m = 30$ ms, and the spiking threshold $v_{\rm th}$ of v is set to 1, while its reset value is $v_r = 0$. Whenever v_i reaches $v_{\rm th}$, neuron i emits a spike and is reset to v_r. In our simulations we set $a = 1.3$, so that neurons are in a spiking regime; i.e., even in the absence of synaptic stimuli they fire periodically, with a period $T_0 = \ln(a/(a-1))$. For the coupling dynamics we use the Tsodyks, Uziel, and Markram model, a description of short-term synaptic plasticity that has been successfully tested in experimental setups [20,21]. According to [22], the dynamics of the synapse between postsynaptic (i.e., receiving) neuron i and presynaptic (i.e., transmitting) neuron j is described in terms of the fraction of its *active*, $y_{ij}(t)$, *available*, $x_{ij}(t)$, and *inactive*, $z_{ij}(t)$, resources. These quantities are assumed to evolve according to the following set of coupled differential equations:

$$\dot{y}_{ij}(t) = -\frac{y_{ij}(t)}{\tau_{\rm in}} + u_{ij}(t)x_{ij}(t)S_j(t), \tag{2}$$

$$\dot{x}_{ij}(t) = \frac{z_{ij}(t)}{\tau_{\rm r}^i} - u_{ij}(t)x_{ij}(t)S_j(t), \tag{3}$$

$$x_{ij}(t) + y_{ij}(t) + z_{ij}(t) = 1, \tag{4}$$

where Eq. (4) is a conservation rule and $S_j(t) = \sum \delta(t - t_j(n))$ is the spike train of presynaptic neuron j emitting its nth pulse at time $t_j(n)$. Whenever neuron j emits a spike, it activates a fraction u_{ij} of the available resources x_{ij}. In between two consecutive spikes, the fraction of active resources y_{ij} decreases with time, with a time constant $\tau_{\rm in}$, and the fraction of available resources recovers in a time $\tau_{\rm r}^i$ the fraction of inactive resources z_{ij}. If postsynaptic neuron i is inhibitory, the recovery time is much shorter. In particular, the typical phenomenological values are $\tau_{\rm in} = 0.2$, while $\tau_{\rm r}^i = 3.4$ if i is inhibitory and $\tau_{\rm r}^i = 26.6$ if i is excitatory. Moreover, if the index i corresponds to an excitatory neuron, $u_{ij}(t)$ is assumed to be constant, namely, $u_{ij} = U = 0.5$; otherwise,

$$\dot{u}_{ij}(t) = -\frac{u_{ij}(t)}{\tau_{\rm f}} + U_f(1 - u_{ij}(t))S_j(t), \tag{5}$$

where $\tau_{\rm f} = 33.25$ is the facilitation time scale and $U_f = 0.08$ is a phenomenological parameter [22,23].

The Tsodyks-Uziel-Markram model equations combine depressive and facilitating mechanisms of plasticity [22]. If the postsynaptic neuron is excitatory, the mechanism is purely depressive, as a high-frequency spiking of presynaptic neurons delays the available synaptic resources. If the postsynaptic neuron is inhibitory, the dynamics of u_{ij} describes a facilitating mechanism, reinforcing the synapse when presynaptic neuron j has high electric activity. Equations (2)–(5) participate in the neural network dynamics by specifying in Eq. (1) the form of the synaptic current received by neuron i:

$$I_i^{\rm syn}(t) = \frac{g}{N}\sum_{j\neq i} \epsilon_{ij} y_{ij}(t), \tag{6}$$

where g is the coupling parameter and the index j labels the presynaptic neurons of neuron i. The matrix elements ϵ_{ij} can take the values 0, 1, and -1 if, respectively, presynaptic neuron j is disconnected, excitatory, or inhibitory with respect to postsynaptic neuron i. In our first approach, we consider random uncorrelated dense networks, i.e., networks where any correlation among different degrees is absent, and the degree is proportional to N [this explains the normalization factor $1/N$ in Eq. (6)].

By denoting $\tilde{k} = k/N$ the rescaled in-degree, where $k \in [0, N-1]$ is the number of in-connections of a given neuron, we can associate with the uncorrelated network its in-degree distribution $P(\tilde{k})$. In general, inhibitory and excitatory neurons may have different in-degree distributions, $P_I(\tilde{k})$ and $P_E(\tilde{k})$. In particular, $P_I(\tilde{k})$ and $P_E(\tilde{k})$ are the probabilities that an inhibitory and an excitatory neuron receive $\tilde{k}N$ inputs from other neurons. In this setup, we fix the in-degree distributions of inhibitory and excitatory neurons, assuming that typically they have randomly distributed outputs.

III. HETEROGENEOUS MEAN FIELD FOR A NETWORK OF EXCITATORY AND INHIBITORY NEURONS

The HMF approach (see [18] and [19]) amounts to setting a thermodynamic limit while keeping the neuron in-degree density $\tilde{k}$ fixed. Dynamics (1) is replaced by an evolution rule for *classes* of neurons labeled by their $\tilde{k}$,

$$\dot{v}_{\tilde{k}}(t) = a - v_{\tilde{k}}(t) + g\tilde{k}Y(t), \tag{7}$$

where $Y(t)$ is the average synaptic activity field. In [18] and [19] this method was applied to dense uncorrelated networks of excitatory LIF neurons, and it revealed a very good approximation of dynamics (1) for any large finite network. For instance, the HMF approach is effective also for sparse uncorrelated networks, provided they exhibit a sufficiently large average in-degree [19].

Here we describe how the HMF approach can be extended to networks of inhibitory and excitatory neurons. In this case, the dynamics of each neuron depends on the number of its inhibitory and excitatory presynaptic neurons. The information is stored in the adjacency matrix ϵ_{ij}, which encodes the network topology. Following the HMF strategy, we split the dynamics, (7), into two equations for classes of excitatory (E) and inhibitory (I) postsynaptic neurons with in-degree density $\tilde{k}$:

$$\dot{v}^E_{\tilde{k}}(t) = a - v^E_{\tilde{k}}(t) + g\tilde{k}(-f_I Y_{EI}(t) + f_E Y_{EE}(t)), \tag{8}$$

$$\dot{v}^I_{\tilde{k}}(t) = a - v^I_{\tilde{k}}(t) + g\tilde{k}(-f_I Y_{II}(t) + f_E Y_{IE}(t)). \tag{9}$$

The last expressions on the right-hand side of these equations correspond to the average synaptic activity fields received by postsynaptic E and I neurons with label $\tilde{k}$ from their presynaptic E and I neurons. The fractions of inhibitory and excitatory neurons are denoted f_I and $f_E = 1 - f_I$, respectively.

These equations determine the spike trains $S^I_{\tilde{k}}(t)$ and $S^E_{\tilde{k}}(t)$ of inhibitory and excitatory classes of neurons, with in-degree density $\tilde{k}$. The spike trains enter the set of Eqs. (2)–(4), which splits into four sets, identified by the superscript $(\dagger,*)$, where both symbols can be either I (inhibitory) or E (excitatory), with $*$ corresponding to presynaptic neurons with label $\tilde{k}$. In formulas

$$\dot{y}^{(\dagger,*)}_{\tilde{k}}(t) = -\frac{y^{(\dagger,*)}_{\tilde{k}}(t)}{\tau_{\rm in}} + u^{(\dagger,*)}_{\tilde{k}}(t)x^{(\dagger,*)}_{\tilde{k}}(t)S^*_{\tilde{k}}(t), \tag{10}$$

$$\dot{x}^{(\dagger,*)}_{\tilde{k}}(t) = \frac{z^{(\dagger,*)}_{\tilde{k}}(t)}{\tau_{\rm r}^{\dagger}} - u^{(\dagger,*)}_{\tilde{k}}(t)x^{(\dagger,*)}_{\tilde{k}}(t)S^*_{\tilde{k}}(t), \tag{11}$$

$$x^{(\dagger,*)}_{\tilde{k}}(t) + y^{(\dagger,*)}_{\tilde{k}}(t) + z^{(\dagger,*)}_{\tilde{k}}(t) = 1, \tag{12}$$

where $u^{(\dagger,*)}_{\tilde{k}} = U$ if $\dagger = E$, and otherwise,

$$\dot{u}^{(\dagger,*)}_{\tilde{k}}(t) = -\frac{u^{(\dagger,*)}_{\tilde{k}}(t)}{\tau_{\rm f}} + U_f(1 - u^{(\dagger,*)}_{\tilde{k}}(t))S^*_{\tilde{k}}(t). \tag{13}$$

Note that the value of the parameter $\tau_{\rm r}^{\dagger}$ depends on the type of the postsynaptic neuron.

These equations can be closed by the consistency relations defining the average fields that appear in Eqs. (8) and (9):

$$Y_{\dagger,*} = \int_0^1 P_*(\tilde{k}) y^{(\dagger,*)}_{\tilde{k}} d\tilde{k}. \tag{14}$$

In the following, it is also convenient to define the global average fields, Y_I and Y_E, received by inhibitory and excitatory neurons:

$$Y_I = -f_I Y_{II}(t) + f_E Y_{IE}, \tag{15}$$

$$Y_E = -f_I Y_{EI}(t) + f_E Y_{EE}. \tag{16}$$

IV. DYNAMICAL EFFECTS OF INHIBITORY NEURONS

In a series of papers [18,19,24,25] we have analyzed in detail the dynamics of random, uncorrelated, dense networks of excitatory LIF neurons and successfully compared it with the corresponding HMF dynamics. Analogously, in this section, we provide a short summary of some basic dynamical regimes of the HMF dynamics with inhibition presented in Sec. III.

To appreciate the reliability of this approach, we preliminarily give a comparison between the HMF method and direct numerical simulations, performed on a large finite network made up of $N = 5000$ neurons. In Fig. 1 we plot the average interspike time interval ($\overline{\rm ISI}_{\tilde{k}}$) of each neuron as a function of its in-degree density $\tilde{k}$. Data have been obtained for the Gaussian probability distributions $P_I(\tilde{k})$ and $P_E(\tilde{k})$ of $\tilde{k}$, with

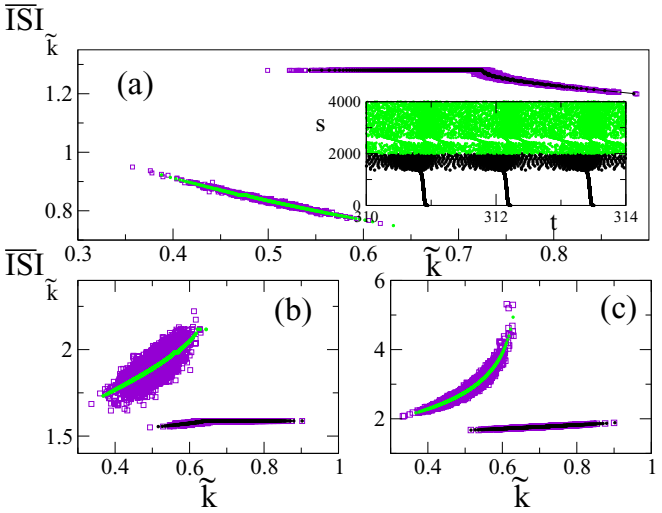

FIG. 1. Average interspike time interval ($\overline{\rm ISI}$) for a network of $N = 5000$ neurons [(purple) squares] as a function of the in-degree density $\tilde{k}$. The distributions $P_I(\tilde{k})$ and $P_E(\tilde{k})$ are both Gaussian, with $\langle\tilde{k}_I\rangle = 0.5$, $\langle\tilde{k}_E\rangle = 0.7$, $\tilde{\sigma}_I = 0.04$, and $\tilde{\sigma}_E = 0.056$, respectively. (a) The inhibitory fraction $f_I = 0.1$; (b) $f_I = 0.65$; (c) $f_I = 0.85$. Black (excitatory neurons) and green (inhibitory neurons) dots were obtained by the corresponding HMF dynamics. Note the plateau region typical of the population of excitatory neurons, which is almost absent for the population of inhibitory neurons. Inset: Raster plot of the HMF dynamics, where the neuron index s is ordered according to the in-degree density $\tilde{k}$ (see text): black dots, excitatory neurons ($0 < s \leqslant 2000$); green dots, inhibitory neurons.

$\langle \tilde{k}_I \rangle = 0.5$, $\langle \tilde{k}_E \rangle = 0.7$, and standard deviations $\tilde{\sigma}_I = 0.04$ and $\tilde{\sigma}_E = 0.056$. Here and in the following, we have assumed the phenomenological values of the parameters $\tau_f = 33.25$ and $g = 30$ (see [22] and [23]). In Fig. 1 we have chosen three values of the inhibitory fraction, $f_I = 0.1$, $f_I = 0.65$, and $f_I = 0.85$, the first two corresponding to synchronous regimes and the last to an asynchronous one. The matching between the HMF method and the direct simulations is remarkable in all regimes. The HMF dynamics has been implemented by sampling $\tilde{k}$ with 2000 values for both groups of neurons. As expected, the fluctuations are much smaller in the HMF case. This confirms the numerical efficiency of the method with respect to the direct simulation of a finite massive network. In particular, the method already provides a quite accurate description of the dynamics in the thermodynamic limit for a sampling of $P(k)$ by a few hundred bins (see [19] for an extensive discussion of the efficiency of the HMF approach).

Let us now consider in detail the case $f_I = 0.1$, corresponding to Fig. 1(a). As observed in fully excitatory networks [18,19,25], excitatory neurons split into two families, namely, periodic (locked) and aperiodic (unlocked) neurons, corresponding to $\tilde{k} < \langle \tilde{k}_E \rangle$ and to $\tilde{k} > \langle \tilde{k}_E \rangle$, respectively. Inhibitory neurons cover an approximately uniform range of higher frequencies. In the inset we report the raster plot (i.e., index of the neuron s vs its firing times t) of the HMF dynamics to point out the microscopic organization of neurons. Excitatory neurons correspond to $0 \leqslant s \leqslant 2000$ (s has been ordered according to decreasing values of $\tilde{k}$). The quasisynchronous bursts observed for $0 \leqslant s < 1300$ are produced by the *locked* excitatory neurons in the plateau region. The *unlocked* neurons ($1300 \leqslant s < 2000$) exhibit irregular firing behavior, as well as most of the inhibitory neurons, which fire more frequently thanks to the facilitation mechanism typical of their synaptic activity. Only a small fraction of inhibitory neurons, around $\tilde{k} \simeq 4.7$, produces quasisynchronous bursts, but at a different pace with respect to the excitatory ones. Despite the complexity of the raster plot in this regime, the average activity fields $Y_E(t)$ and $Y_I(T)$ exhibit periodic oscillations, which characterize a dynamical phase with a high level of synchrony [e.g., see the inset in Fig. 3(a)]. In particular, the frequency of the fields coincides with the frequency of the locked excitatory neurons, while excitatory and inhibitory unlocked neurons exhibit a quasiperiodic behavior, as discussed in [25]. Finally, locked inhibitory neurons display an ISI in a simple rational relation with the period of the field (2/3 for the case illustrated in Fig. 1). In other words, we are facing a sort of high-order locking effect induced by the global fields $Y_I(T)$ in a subset of inhibitory neurons with a proper frequency.

We now report on how the dynamical regime of the HMF dynamics of the model in Fig. 1 changes as a function of the fraction f_I of inhibitory neurons. As pointed out in [26], an effective order parameter for exploring the HMF phase diagram is the extremal values of $Y_E(t)$. For increasing values of f_I, the amplitude of $Y_E(t)$ decreases and the synchrony mechanisms within the network are significantly modified. In Fig. 2 we plot the maximum (filled circles) and minimum (asterisks) values of $Y_E(t)$ as a function of f_I. One can distinguish three main regimes. For $0 < f_I < 0.45$ (regime A), the network dynamics is driven by locked excitatory neurons. Figure 3(a) shows the average ISI as a function of $\tilde{k}$ for

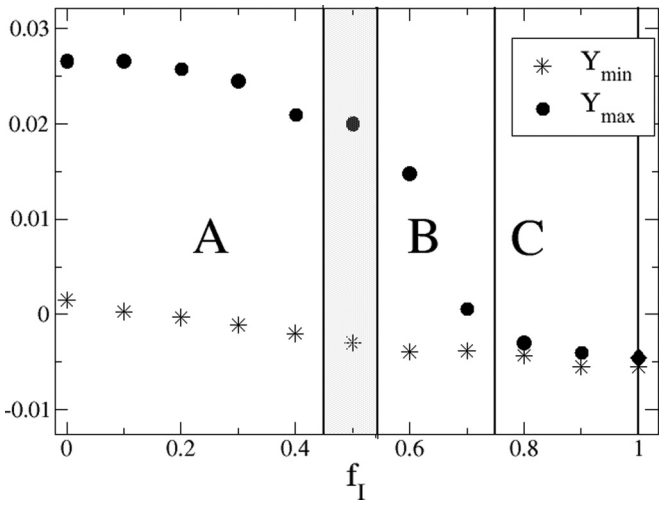

FIG. 2. Maximum (filled circles) and minimum (asterisks) values of the global field $Y_E(t)$ as a function of the fraction of inhibitory neurons f_I obtained from the HMF dynamics. The distributions $P_{E/I}(\tilde{k})$ and the HMF sampling adopted are the same as in Fig. 1.

$f_I = 0.2$. We see that a large portion of the excitatory neurons is locked in phase, yielding the quasisynchronous events appearing also in the inset in Fig. 1. The inhibitory neurons are mainly unlocked and they fire at a higher frequency. In the inset we plot the average activity fields received by excitatory and inhibitory neurons, $Y_E(t)$ and $Y_I(t)$. Both fields take positive values, while $Y_I(t) > Y_E(t)$, as a consequence of the facilitation mechanism, which increases the synaptic efficiency during fast firing activity.

For $f_I > 0.7$ (regime C), $Y_E(t)$ becomes negative and its amplitude decreases significantly, while neither $Y_E(t)$ nor $Y_I(t)$ exhibits any oscillating behavior (not shown). This dynamical phase is dominated by inhibitory neurons and the natural firing activity of all neurons slows down to an irregular behavior, where quasisynchronous events disappear.

For $0.55 < f_I < 0.7$ (regime B) partial synchronization with quasisynchronous events persists, as in regime A. On the other hand, the microscopic organization of firing events is different, as shown in Fig. 3(b), where $f_I = 0.6$. Looking at the inset, one observes that inhibitory neurons receive a relatively higher-amplitude activity field, $Y_I(t)$, with respect to excitatory neurons, $Y_E(t)$. The main distinctive feature with respect to regime A is that both $Y_E(t)$ and $Y_I(t)$ also take negative values, and inhibitory neurons are no faster than excitatory ones, as clearly illustrated by the average ISI *vs* $\tilde{k}$. In particular, an appreciable subset of inhibitory neurons locks at the same frequency as the *locked* excitatory ones (see the initial plateau around $\tilde{k} = 0.4$). As for the *unlocked* inhibitory neurons, they fire at lower frequencies than the excitatory ones, which, on their side, are *locked* for large values of $\tilde{k}$ [compare Figs. 3(a) and 3(b)]. Finally, also in this case inhibitory neurons may display a higher-order locking. In particular, the low-frequency plateaus are characterized by an ISI which is in a simple rational relation with the period of the global field, i.e. the ISI of locked excitatory neurons.

At the edge between regime A and regime B, there is a region of *optimal synchronization* (vertical gray band in Fig. 2),

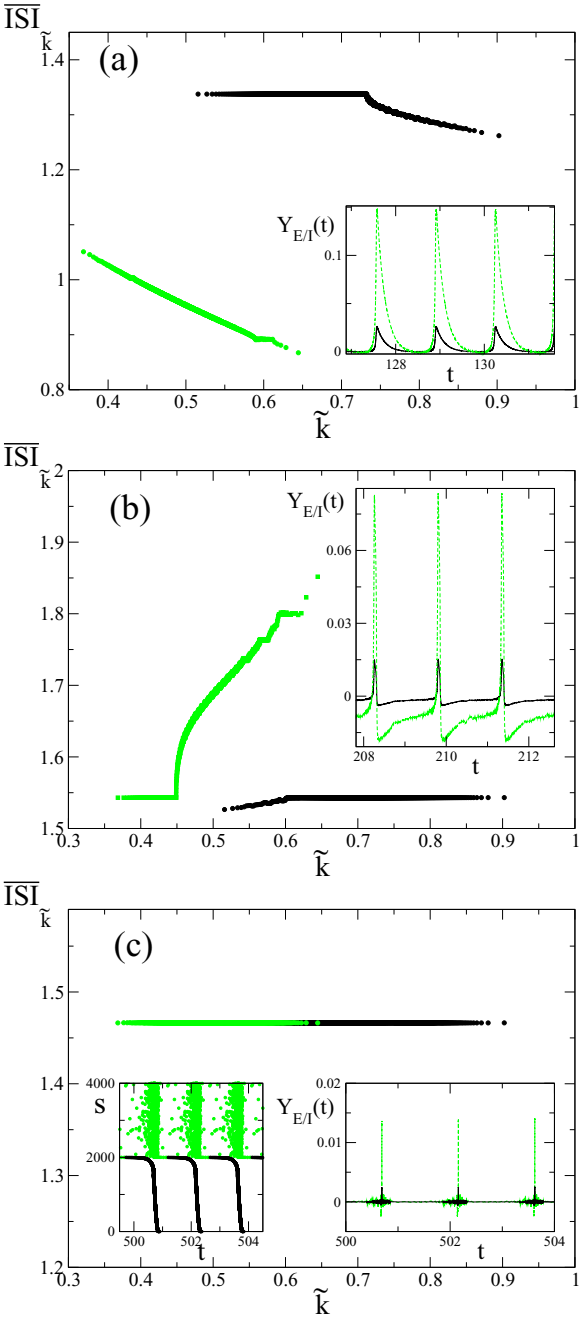

FIG. 3. Dynamical regimes for different values of the fraction of inhibitory neurons f_I for the same model as in Fig. 1. The dependence of the average $\overline{\mathrm{ISI}}_{\tilde{k}}$ on $\tilde{k}$ for (a) $f_I = 0.2$, (b) $f_I = 0.6$, and (c) $f_I = 0.5$. Green dots, inhibitory neurons; black dots, excitatory neurons. Insets: Average activity fields $Y_E(t)$ (solid black lines) and $Y_I(t)$ [dashed (green) lines]. Left inset in (c): Raster plot of firing events. As in the inset in Fig. 1, black dots represent excitatory neurons; green dots, inhibitory neurons.

where neither excitatory nor inhibitory neurons prevail. The dynamics typical of this region is shown in Fig. 3(c), where $f_I = 0.5$. The average ISI is independent of $\tilde{k}$. This means that all neurons fire at a common frequency very close to $1/T_0$, i.e., the frequency of the noninteracting system ($g = 0$); only their relative phases depend on $\tilde{k}$. Notwithstanding this, the microscopic organization of firing events is still quite complex: as shown in the raster plot in the left inset, there is a majority of inhibitory and excitatory neurons participating in the same quasisynchronous events; i.e., they are almost in phase. The right inset shows that $Y_E(t)$ and $Y_I(t)$ exhibit periodic fluctuations of very low amplitude (i.e., $g \approx 0$), apart from narrow activity peaks, which correspond to the quasisynchronous events shown in the left inset. This is quite interesting collective dynamical behavior, emerging in a weakly interacting network, where the complex organization of the phases of equally periodic excitatory and inhibitory neurons is determined by the random structure of the network, i.e., by the in-degree density distributions $P_E(\tilde{k})$ and $P_I(\tilde{k})$.

V. RELATION BETWEEN AVERAGE EXCITATORY AND INHIBITORY ACTIVITY FIELDS

The HMF approach provides also the possibility of working out an analytic study of the complex network dynamics described in the previous section. For instance, direct inspection of Fig. 3 suggests that the average synaptic activity fields defined in Eqs. (15) and (16) exhibit quite similar behavior with time, despite single inhibitory and excitatory neurons receiving different synaptic activity fields and emitting different spike trains. In Fig. 4 we focus on the time evolution of $Y_E(t)$ and $Y_I(t)$ for the HMF with $f_I = 0.1$ (see Fig. 4 caption for details). Apart from small fluctuations, the two fields coincide by a suitable rescaling of their amplitudes (see left inset). An analytic estimate of the rescaling factor can be obtained by a heuristic argument. Since Y_E and Y_I depend on the fields $y_{\tilde{k}}^{(E,*)}$ and $y_{\tilde{k}}^{(I,*)}$, respectively [see Eq. (14)], their difference can be traced back to the different dynamical behavior of $u_{\tilde{k}}^{(\dagger,*)}$ [see Eq. (13)], which comes into play in the firing events.

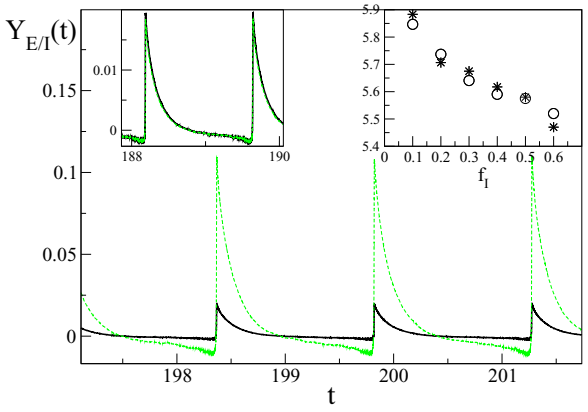

FIG. 4. Time evolution of $Y_I(t)$ [dashed (green) line] and $Y_E(t)$ (solid black line) for the HMF dynamics with $f_I = 0.1$. Left inset: $Y_I(t)$ has been rescaled using the common period of the global fields and the factor obtained analytically (see text). Right inset: Comparison between the scale factor deduced from simulations (black circles) and the one obtained analytically (asterisks). The latter was calculated by dividing the right-hand-side term in Eq. (17) by the right-hand-side term in Eq. (18), where the period T was obtained from the time evolution of the global fields. The distributions $P_{E/I}(\tilde{k})$ and the HMF sampling adopted are the same as in Fig. 1.

Accordingly, in between two spikes, $Y_I(t)$ and $Y_E(t)$ follow the same dynamics, i.e., an exponential decay with the same time constant $\tau_{\rm in}$. Let us consider a neuron that, firing its spike train, generates postsynaptic fields $y_{\tilde{k}}^{\dagger,*}(t)$ and assume that it emits spikes at a constant rate; i.e., its synaptic activity field is periodic, with the same period T of the average activity field (actually, locked neurons display this behavior). By imposing the periodicity properties on Eqs. (10) and (13), i.e., $y_{\tilde{k}}^{\dagger,*}(t) = y_{\tilde{k}}^{\dagger,*}(t+T)$, we can obtain an explicit expression of their time dependence. Both fields exhibit the same exponential decay, with time constant $\tau_{\rm in}$, and their amplitudes are found to depend on the different boundary conditions during firing events for excitatory and inhibitory neurons. In formulas we report their maximum values, $\tilde{y}_{\tilde{k},\rm MAX}^{E,*}$ and $\tilde{y}_{\tilde{k},\rm MAX}^{I,*}$, achieved immediately after spike emission:

$$\tilde{y}_{\tilde{k},\rm MAX}^{E,*} = \frac{U}{1-(1-U)e^{-\frac{T}{\tau_{\rm in}}} + U\frac{\tau_{\rm r}^E}{\tau_{\rm r}^E-\tau_{\rm in}}\frac{e^{-\frac{T}{\tau_{\rm r}^E}}-e^{-\frac{T}{\tau_{\rm in}}}}{1-e^{-\frac{T}{\tau_{\rm r}^E}}}}, \tag{17}$$

$$\tilde{y}_{\tilde{k},\rm MAX}^{I,*} = \frac{\tilde{u}^I}{1-(1-\tilde{u}^I)e^{-\frac{T}{\tau_{\rm in}}} + \tilde{u}^I\frac{\tau_{\rm r}^I}{\tau_{\rm r}^I-\tau_{\rm in}}\frac{e^{-\frac{T}{\tau_{\rm r}^I}}-e^{-\frac{T}{\tau_{\rm in}}}}{1-e^{-\frac{T}{\tau_{\rm r}^I}}}}, \tag{18}$$

$$\tilde{u}^I = U_f\frac{e^{-\frac{T}{\tau_f}}}{1-e^{-\frac{T}{\tau_f}}+U_f e^{-\frac{T}{\tau_f}}}. \tag{19}$$

Note that, as the two fields decrease exponentially with the same time constant in between two consecutive spikes, the field $\tilde{y}_{\tilde{k}}^{E,*}(t)$ is equal to $\tilde{y}_{\tilde{k}}^{I,*}(t)$ apart from a scaling factor that can be calculated at their maximum values, obtained from Eqs. (17) and (18). In the right inset in Fig. 4 we compare the scaling factor computed numerically with the analytic prediction obtained from Eqs. (17)–(19). The agreement is quite good, despite the simplifying assumptions introduced in the analytic estimate. Let us point out that, in principle, the proportionality assumption should hold for a dynamics where all the neurons display the same periodic behavior. Simulations indicate that this agreement is still effective when the frequencies of most neurons are not too different from the frequency of the average activity fields $Y_E(t)$ and $Y_I(t)$. This is indeed shown in Fig. 3, where the value of the ISI between the different neurons varies by, at most, a factor of 1.5.

On the other hand, there are situations where such a quasiproportionality fails. For instance, if a significant fraction of neurons is subcritical ($a < 1$), this condition cannot be achieved since the global activity fields are no more periodic. In Fig. 5 we report the results of numerical simulations for a neural network, where the values of stimulus a attributed to individual neurons are extracted from a uniform probability distribution $P(a)$ with average value $\bar{a} < 1$ and support length Δ_a. By choosing the parameters in such a way that approximately half of the neurons are subcritical [Fig. 5(a)], the quasiproportionality of the activity fields is preserved. Conversely, for a slightly smaller value of $\bar{a}$ [see Fig. 3(b)], neural activity is highly reduced and there is no more space for quasiperiodic firing events, while the activity fields are no longer proportional.

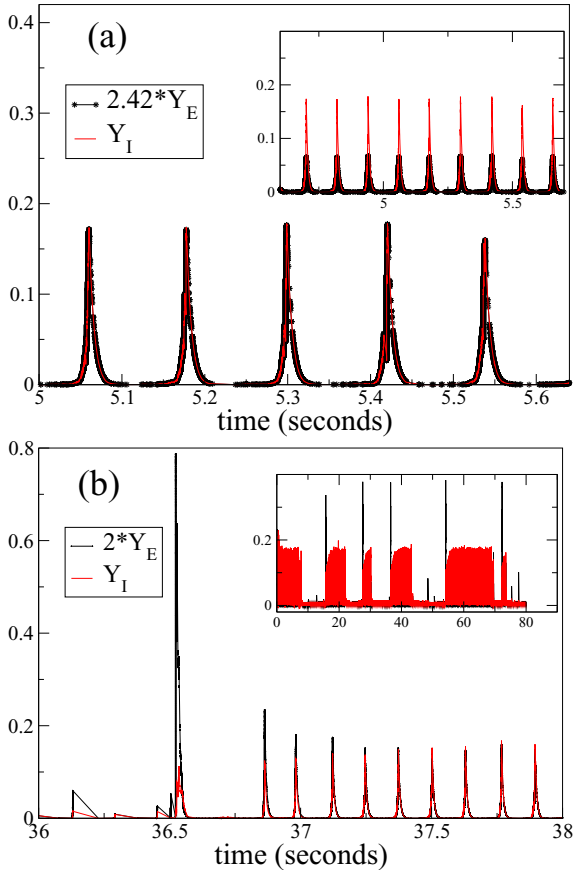

FIG. 5. Time trace of Y_E and Y_I, rescaled by the proportionality scaling. (a) $\bar{a} = 0.9561$; (b) $\bar{a} = 0.9541$. The variance of the uniform distribution is the same: $\Delta_a = 0.1001$. In (a) we have used the scaling deduced by the analytic argument. In (b), since the signals are no longer periodic, Eqs. (17)–(19) do not apply and the best scaling factor minimizing the differences between the fields demonstrates that there is no proportionality. Inset: Data without rescaling.

VI. THE INVERSE PROBLEM WITH INHIBITORY NEURONS

Global synaptic activity fields in extended regions of the brain can be more accessible to experimental measurements than single-neuron activities. As shown in two previous papers [18,19], in the HMF frame one can recover the degree distribution of a fully excitatory LIF network from the knowledge of its global synaptic activity field. In other words, the HMF formulation allows one to solve a global inverse problem. Here we discuss how to extend this result to networks made up of inhibitory and excitatory LIF neurons. The method can be extended to networks with different single-neuron models.

Let us assume that we have access to the measure of the average activity field received by neurons, i.e., $Y(t) = f_E Y_E(t) + f_I Y_I(t)$. We will recover, within a reasonable accuracy, $P_E(\tilde{k})$, $P_I(\tilde{k})$, and f_I, i.e., the probability distributions of the equivalent in-degree density $\tilde{k}$ of excitatory and inhibitory neurons, as well as their fraction. The procedure is comprised of the following steps.

(i) As discussed in Sec. V, $Y_E(t)$ and $Y_I(t)$ can be rescaled by a suitable proportionality constant, γ, whose explicit expression depends only on phenomenological parameters of the model [see Eqs. (17)–(19)]. Accordingly, we can write

$$Y_I(t) = \gamma Y_E(t) = \frac{\gamma Y(t)}{1 + (\gamma - 1) f_I}, \tag{20}$$

and we consider $Y_E(t)$ and $Y_I(t)$ to be functions of $Y(t)$ and of the unknown fraction f_I.

(ii) For each value of f_I, we integrate the dynamics, (8) and (9), that produce the spike trains $S^*_{\tilde{k}}(t)$ that allow us to integrate Eqs. (10)–(13).

(iii) We use $\mathsf{y}^{(\dagger,*)}_{\tilde{k}}(t, f_I)$ to impose the self-consistency condition [see (14)]:

$$\tilde{Y}_{\dagger *}(t) = \int_0^1 P_*(\tilde{k}) \mathsf{y}^{(\dagger,*)}_{\tilde{k}}(t, f_I) d\tilde{k}. \tag{21}$$

We can write the equations analogous to (15) and (16),

$$\tilde{Y}_I = -f_I \tilde{Y}_{II}(t) + f_E \tilde{Y}_{IE}, \tag{22}$$

$$\tilde{Y}_E = -f_I \tilde{Y}_{EI}(t) + f_E \tilde{Y}_{EE}, \tag{23}$$

and

$$\tilde{Y}(t) = f_E \tilde{Y}_E(t) + f_I \tilde{Y}_I(t).$$

(iv) Note that the effective field $\tilde{Y}(t)$ depends on the quantities to be recovered, namely, $P_E(\tilde{k})$, $P_I(\tilde{k})$, and f_I, and the self-consistency condition, (21), should hold only if $\tilde{Y}(t) \to Y(t)$. In practice, a suitable estimate of the unknown quantities can be obtained by minimizing the variance,

$$\sigma^2 = \frac{1}{t_1 - t_0} \int_{t_0}^{t_1} (\tilde{Y}(t) - Y(t))^2 dt, \tag{24}$$

where $[t_0, t_1]$ is the measurement time interval of $Y(t)$. The minimization procedure can be achieved using a zero-temperature Montecarlo algorithm, as for the purely excitatory case (see [18]).

The inverse problem procedure, (i)–(iv), allows us to recover quite well the fraction $f_I = 0.1$ of inhibitory neurons. In Fig. 6 we show the reconstruction of $P_E(\tilde{k})$ and $P_I(\tilde{k})$ for the dynamics reported in Fig. 1. This analysis confirms that, in the case of Gaussian in-degree density distributions for both excitatory and inhibitory neurons, the average synaptic activity signal can be efficiently inverted. The bumps appearing in the reverse estimate of the degree distribution of inhibitory neurons are just effects of the adopted numerical accuracy, which could be improved by considering longer time spans and a finer sampling of $\tilde{k}$.

Interestingly, this global inverse procedure can be applied also to the case of broad power-law distributions, with inhibitory neurons typically displaying higher connectivities [9]. As an example, here we report just the case of a network with $f_I = 0.3$ where $P_E(\tilde{k})$ and $P_I(\tilde{k})$ are power-law distributions, scaling as $\tilde{k}^{-\alpha}$ [8]. In order to avoid too small values of $\tilde{k}$ we impose a lower cutoff, $\tilde{k}^E_m$ and $\tilde{k}^I_m$, on both probability distributions, which are accordingly normalized.

In Fig. 7 we report the results of the inverse problem procedure. The average synaptic activity field $Y(t)$ has been computed from the dynamics of a finite network of $N = 5000$ neurons. Figures 7(a) and 7(b) show the reconstruction of $P_E(\tilde{k})$ and $P_I(\tilde{k})$. The minimization procedure [step (iv)] provides quite an accurate reconstruction of the fraction $f_I \approx 0.3$ and of the distribution $P_E(\tilde{k})$ over the whole range of definition, while $P_I(\tilde{k})$ is recovered just for $\tilde{k} \geqslant \tilde{k}^I_m$. This result indicates that a more refined algorithm should be employed to improve the quality of the inversion.

We remark that, although in this case the reconstruction of $P_I(\tilde{k})$ is not completely reliable, the presence of a fraction of inhibitory neurons in the inversion procedure is crucial also

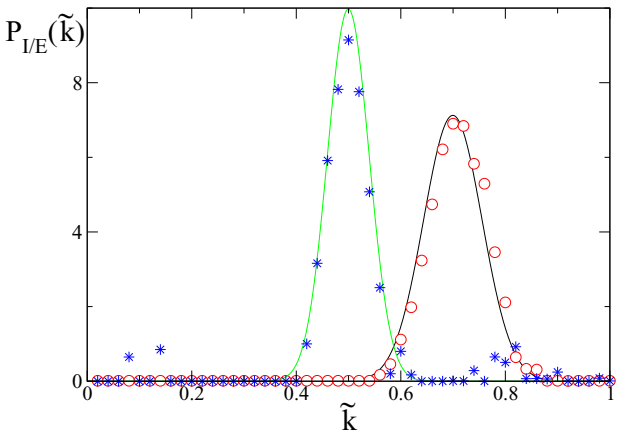

FIG. 6. Reconstruction of $P_E(\tilde{k})$ and $P_I(\tilde{k})$ for the network in Fig. 1. Solid curves are the expected distributions, while (red) circles (excitatory neurons) and (blue) asterisks (inhibitory neurons) are the reconstructions obtained with the self-consistent inversion equation.

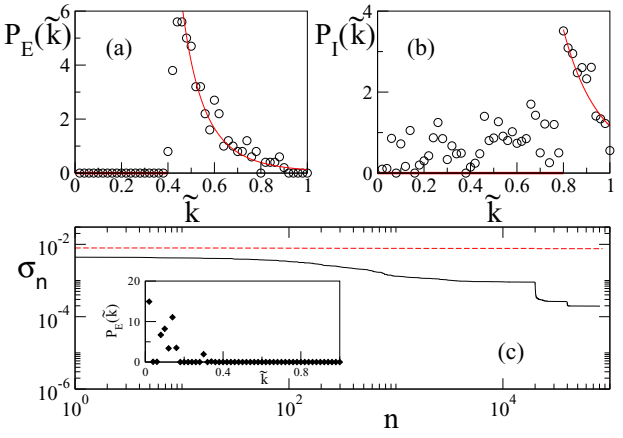

FIG. 7. Reconstruction with power-law connectivity degree distributions. Reconstructions of (a) $P_E(\tilde{k})$ and (b) $P_I(\tilde{k})$ (black circles). The fraction of inhibitory neurons proves to be $f_I = 0.3$, as wanted. The solid (red) line is the power-law $\tilde{k}^{-5}$ with cutoff $\tilde{k}^I_m = 0.8$ and $\tilde{k}^E_m = 0.4$. (c) The procedural result when the global field is inverted by considering only excitatory neurons; n is the MC step. In particular, we compare the convergence of the parameter σ in the case of (a) and (b), where the presence of inhibitory neurons is taken into account (solid black line), with that in the case where the inverse problem has been performed by considering only the excitatory population [dashed (red) line]. Inset: The reconstructed $P_E(\tilde{k})$ in the latter case. We see that it is quite far from the expected one in (a).

for the reconstruction of the excitatory distribution. Let us consider the global field and implement the inverse problem in the absence of inhibitory neurons (actually the procedure reported in [18]). In Fig. 7(c), we can observe that, by omitting the presence of an inhibitory population, the reconstruction of the network structure yields a bad regeneration of $P_E(\tilde{k})$ as well (see the inset). Moreover, we compare the reconstruction performance by plotting the convergence of σ in the Monte Carlo minimization. The curve, in the presence of only excitatory neurons, converges to higher values of σ. More precisely, the relative error $\delta = \sigma/\langle Y \rangle$, which is 48% in the case without inhibitory neurons, reduces to 1% when inhibitory neurons are taken into account. This implies that the matching between $\tilde{Y}(t)$ and $Y(t)$ is neatly improved by considering the inhibitory population.

VII. CONCLUSIONS AND PERSPECTIVES

We have studied the dynamics of random uncorrelated dense networks of LIF neurons with inhibitory and excitatory components by the HMF approximation. This method proves extremely effective in reproducing the complex emerging dynamical phases of the system and provides significative advantages, both in numerical simulations and in the analytic approach to the inverse problem, which can be formulated in terms of average properties.

The model presents a very rich dynamical phase diagram where inhibitory and excitatory components feature different complex evolutions. This complexity does not restrain the HMF approach from offering an interesting first insight into the global dynamics, which can be grasped directly from a simplified version of the HMF equations. Precisely, if the dynamics of the two types of synapses were the same, the presence of a certain fraction f_I of inhibitory neurons could be described by introducing an effective in-degree density distribution.

Indeed, since in this simple case the same activity fields are transmitted to inhibitory and excitatory neurons, we deal with just a single set of evolution equations, where the dependence on the inhibitory or excitatory nature of presynaptic and postsynaptic neurons can be omitted. In fact, any neuron with degree $\tilde{k}$ receives a field $g\tilde{k}Y$, where

$$Y = \int_0^1 [f_E P_E(\tilde{k}) - f_I P_I(\tilde{k})] y_{\tilde{k}}(t) d\tilde{k}.$$

If the term in brackets has a definite sign, the network is equivalent to a completely inhibitory or excitatory (depending on the sign) network with an effective probability distribution $F(\tilde{k}) = |f_E P_E(\tilde{k}) - f_I P_I(\tilde{k})|$. In particular, if $P_E = P_I$, the introduction of a fraction of inhibitory neurons f_I is equivalent to an *effective dilution* in the original network, obtained through $2f_I$ cuts of the links. If the term in brackets has no definite sign, $F(\tilde{k})$ is not a probability distribution, so that the real dynamics does not correspond to an equivalent excitatory or inhibitory network.

In the more complex case considered in this paper, the inhibitory dynamics is characterized by a facilitation effect and the field received by inhibitory neurons turns out to be larger than the excitatory field. This difference can be approximately estimated by an analytic argument, which allows us to implement an approximated inverse problem for the distributions $P_*(\tilde{k})$ even in the presence of inhibition.

The global inverse problem proves very effective in reproducing the in-degree density probability distributions of the two populations, together with the fraction of inhibitory neurons, for meaningful distributions ranging from Gaussians to power laws. On technical grounds, the inversion could be improved by adopting more refined minimization procedures, but it is significant that even the simple zero-temperature Monte Carlo method adopted here is sufficient to provide the wanted outcome.

This result paves the way to an analysis of experimental data on the average synaptic activity fields in broad regions of the brain. Moreover, the overall approach can be extended to models of correlated dense networks with single-neuron dynamics different from LIF.

ACKNOWLEDGMENT

The authors would like to warmly thank L. De Arcangelis for useful suggestions and discussions and for the constant stimulation to publish, as quickly as possible, the results reported in this paper.

[1] S. Royer and D. Paré, Nature **422**, 518 (2003).
[2] M. N. Shadlen and W. T. Newsome, J. Neurosci. **18**, 3870 (1998).
[3] A. M. Sillito, J. Physiol. **250**, 305 (1975).
[4] M. Wallace *et al.*, Neuron **74**, 793 (2012).
[5] B. Tahvildari *et al.*, J. Neurosci. **32**, 12165 (2012).
[6] N. Brunel, J. Comput. Neurosci. **8**, 183 (2000).
[7] C. R. Noback *et al.*, *The Human Nervous System: Structure and Function*, No. 744 (Springer Science & Business Media, Berlin, 2005).
[8] V. Capano, H. J. Hermann, and L. De Arcangelis, Sci. Rep. **5**, 9895 (2015).
[9] P. Bonifazi *et al.*, Science **326**, 1419 (2009).
[10] H. R. Wilson and J. D. Cowan, Biophys. J. **12**, 1 (1972).
[11] C. van Vreeswijk and H. Sompolinsky, Science **274**, 1724 (1996).
[12] D. Amit and N. Brunel, Cerebral Cortex **7**, 237 (1997).
[13] M. Tsodyks *et al.*, J. Neurosci. **17**, 4382 (1997).
[14] L. Calamai, A. Politi, and A. Torcini, Phys. Rev. E **80**, 036209 (2009)
[15] D. Millman, S. Mihalas, A. Kirkwood, and E. Niebur, Nat. Phys. **6**, 801 (2010).
[16] B. Cessac, B. Doyon, M. Quoy, and M. Samuelides, Physica D: Nonlin. Phenom. **74**, 24 (1994).
[17] P. C. Bressloff, Phys. Rev. E **60**, 2160 (1999).
[18] R. Burioni, M. di Volo, M. Casartelli, R. Livi, and A. Vezzani, Sci. Rep. **4**, 4336 (2014).

[19] M. di Volo, R. Burioni, M. Casartelli, R. Livi, and A. Vezzani, Phys. Rev. E **90**, 022811 (2014).
[20] M. Tsodyks and H. Markram, Proc. Natl. Acad. Sci. USA **94**, 719 (1997).
[21] M. Tsodyks, K. Pawelzik, and H. Markram, Neural Comput. **10**, 821 (1998).
[22] M. Tsodyks, A. Uziel, and H. Markram, J. Neurosci. **20**, 825 (2000).
[23] V. Volman, I. Baruchi, E. Persi, and E. Ben-Jacob, Physica A **335**, 249 (2004).
[24] M. di Volo, R. Livi, S. Luccioli, A. Politi, and A. Torcini, Phys. Rev. E **87**, 032801 (2013).
[25] R. Burioni, S. di Santo, M. di Volo, and A. Vezzani, Phys. Rev. E **90**, 042918 (2014).
[26] S. Olmi, R. Livi, A. Politi, and A. Torcini, Phys. Rev. E **81**, 046119 (2010).